Archives of Hydro-Engineering and Environmental Mechanics
Vol. 60 (2013), No. 1–4, pp. 87–105
DOI: 10.2478/heem-2013-0010

VERSITA

Application of an Element-free Galerkin Method to Water Wave Propagation Problems

Ryszard Staroszczyk

Institute of Hydro-Engineering, Polish Academy of Sciences, ul. Kościerska 7, 80-328 Gdańsk, Poland,
e-mail: rstar@ibwpan.gda.pl

(Received October 15, 2013; revised December 20, 2013)

Abstract

The paper is concerned with the problem of gravitational wave propagation in water of variable depth. The problem is solved numerically by applying an element-free Galerkin method. First, the proposed model is validated by comparing its predictions with experimental data for the plane flow in water of uniform depth. Then, as illustrations, results of numerical simulations performed for plane gravity waves propagating through a region with a sloping bed are presented. These results show the evolution of the free-surface elevation, displaying progressive steepening of the wave over the sloping bed, followed by its attenuation in a region of uniform depth. In addition, some of the results of the present model are compared with those obtained earlier by using the conventional finite element method.

Key words: gravity water wave, transient problem, element-free Galerkin method

Notation

$\boldsymbol{b}$	–	body force vector,
c	–	speed of sound,
$\boldsymbol{D}$	–	strain-rate tensor,
g	–	gravity acceleration,
$\boldsymbol{I}$	–	unit tensor,
K	–	fluid compressibility modulus,
N_k	–	shape function,
$\boldsymbol{n}$	–	unit normal vector,
p	–	pressure,
p_j	–	polynomial basis function,
$\boldsymbol{p}$	–	vector of polynomial basis functions p_j,
r	–	distance between two points,
R	–	weighting function support radius,
$\boldsymbol{s}$	–	unit tangential vector,
t	–	time,

$u(\boldsymbol{x}, t)$	–	field function,
$\boldsymbol{v}$	–	velocity vector,
W	–	weighting function,
x_i $(i = 1, 2, 3)$	–	spatial Cartesian coordinates,
$\boldsymbol{x}$	–	position vector,
∇^2	–	Laplace operator,
μ	–	fluid viscosity,
ρ	–	density,
$\boldsymbol{\sigma}$	–	Cauchy stress vector.

1. Introduction

The problem of propagation of free-surface gravitational waves in water of variable depth has been extensively analysed by employing the methods of classical fluid mechanics. Examples of successful treatment of this problem can be found in fundamental works by Stoker (1957), Wehausen and Laitone (1960), and more recently in two volumes of the book by Dingemans (1997). The application of classical analytical solutions, though, especially of those based on a small parameter expansions, is restricted to the cases of small-amplitude waves propagating over beds of small slopes. In situations when we deal with large-amplitude waves and beds of strongly varying geometry, one has usually to resort to discrete methods in order to construct approximate solutions to the problems investigated.

In general, the discrete methods can be divided into two groups. The first group comprises conventional methods, such as the finite difference, finite element and boundary element methods, in which a numerical grid, or mesh, is imposed on the domain of interest, with some (usually regular) pattern of nodal points at which values of unknown functions are calculated. Over the past five–six decades, these methods have proved useful for solving a wide class of problems of computational fluid dynamics. However, the above mesh-based methods fail in many situations of practical importance. For instance, in cases in which complex non-linear phenomena occur, fluid boundaries (free surface or fluid–solid interface) move and change shape rapidly, or fragmentation of fluid takes place. Effective solution of such problems is only possible by means of so-called mesh-free methods, extensively developed in the past two decades. In these new methods the discrete points (or discrete particles) can be irregularly distributed in a domain, and there is no fixed connection among them throughout computations, which gives this approach a great flexibility to deal with problems in which large deformations occur. To this group of methods belong, in particular, the Smoothed Particle Hydrodynamics (SPH) originated by Gingold and Monaghan (1977) and Lucy (1977), and employed to solve fluid dynamics problem by Lo and Shao (2002), Gómez-Gesteira et al (2005), Dalrymple and Rogers (2006) and Antoci et al (2007), or the Finite Point Method (FPM) used by Oñate et al (1996a, b), Löhner et al (2002) and Ortega et al (2007).

In the present work another mesh-free method, namely the Element-Free Galerkin (EFG) method, is applied to solve a gravity water wave transmission problem. The EFG method was formulated in the mid 1990s by Belytschko and co-workers (Belytschko et al 1995, 1996, 1998); some aspects of the method are also discussed in the book by Zienkiewicz and Taylor (2000). Ever since, the EFG method has been successfully used to solve a great number of problems in solid mechanics; however, there have been very few applications of this approach yet in the field of computational hydrodynamics. Therefore, an attempt is made here to fill this gap and to construct an EFG model for fluid flows. The proposed model is employed to analyse the problem of non-linear free-surface waves propagating in water of variable depth. For more generality, the water is treated as a Newtonian viscous and compressible liquid, so that the model can be also used in the future to solve problems encountered in other branches of fluid dynamics.

The numerical EFG model has been used to simulate the plane problems of wave propagation for several cases of simple bed profiles, idealizing the conditions encountered in natural surf zones. First, calculations have been carried out for the flow over the horizontal bed, in order to validate the model by comparing its predictions with experimental data measured in a laboratory flume. Then, the model is employed to simulate the wave transformation in water of variable depth. Two specific cases of the bottom, consisting of horizontal and uniformly sloping segments, are examined. The numerical results illustrate the evolution of the free-surface elevation, displaying gradual steepening of the wave over the sloping bed, followed by its attenuation due to dispersion in a region of constant depth. The predictions of the present (mesh-free) EFG model are compared with the results obtained earlier by applying a conventional (mesh-based) finite element method (Staroszczyk 2009), with the aim to investigate how the EFG model performs against the other, better-established discrete formulation.

The paper is organized as follows. In Section 2 equations describing the behaviour of water, treated as a viscous and compressible fluid, are presented. Next, in Section 3, a summary of the element-free Galerkin methodology is given, in which the main concepts and ideas underlying the method are outlined, the discrete forms of the governing equations are shown, and the numerical techniques employed to solve the ensuing system of algebraic equations are briefly described. The following Section 4 contains the results of the model application to the wave propagation problems, involving a uniform water depth case used for comparisons with experiments, and two specific cases with a sloping bed for illustrations. Finally, some concluding remarks are drawn in Section 5.

2. Problem Statement

A plane fluid flow problem with a free surface, sketched in Figure 1, is considered, in which gravity waves propagate over an uneven, impermeable and rigid bottom.

The problem is analysed in spatial (Eulerian) Cartesian coordinates, with the axis x_1 directed horizontally, and the vertical axis x_2 directed upwards. The bottom, fixed in time, geometry is defined by the function $x_2 = f(x_1)$, and the current position of the free surface is described by the function $x_2 = h(x_1, t)$, with t denoting time. The symbols $\boldsymbol{n}$ and $\boldsymbol{s}$ in Fig. 1 denote unit vectors normal and tangential to the respective boundaries.

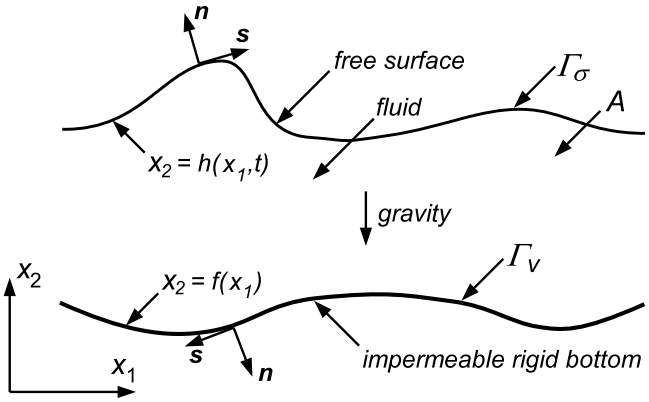

Fig. 1. Plane free-surface fluid flow problem definition

Let the current fluid particle velocity be described by the vector $\boldsymbol{v}$, with components $v_j\,(x_i, t)$, $(i, j = 1, 2)$. Then, the mass conservation law, expressed in the coordinates Ox_i, is given by the continuity equation

$$\frac{\mathrm{D}\rho}{\mathrm{D}t} + \rho \,\mathrm{div}\, \boldsymbol{v} = 0, \tag{1}$$

in which ρ is the fluid density, $\mathrm{D}/\mathrm{D}t$ denotes the material time derivative, and div denotes the spatial divergence operator. The linear momentum conservation balance, in the presence of body forces due to gravity, yields the equation of motion in the form

$$\rho \frac{\mathrm{D}\boldsymbol{v}}{\mathrm{D}t} = \mathrm{div}\, \boldsymbol{\sigma} + \rho \boldsymbol{b}, \tag{2}$$

where $\boldsymbol{\sigma}$ is the Cauchy stress tensor and $\boldsymbol{b}$ denotes the body force vector. In the problem investigated, the latter vector has the components $b_1 = 0$ and $b_2 = -g$, with g being the gravity acceleration.

Water is assumed here to be an isotropic, viscous and compressible fluid, the response of which to stress is defined by the following constitutive relation (Chadwick 1999):

$$\boldsymbol{\sigma} = -\left(p + \frac{2}{3}\mu \,\mathrm{tr}\, \boldsymbol{D}\right)\boldsymbol{I} + 2\mu \boldsymbol{D}. \tag{3}$$

In the above expression, p denotes pressure, μ is the fluid viscosity, $\boldsymbol{I}$ is the unit tensor, tr denotes the trace of a tensor, and $\boldsymbol{D}$ is the strain-rate tensor, with components given by

$$D_{ij} = \frac{1}{2}\left(\frac{\partial v_i}{\partial x_j} + \frac{\partial v_j}{\partial x_i}\right), \quad (i, j = 1, 2). \tag{4}$$

Substitution of the stress relation (3) into the equation of motion (2) results in the Navier-Stokes equation expressed by

$$\rho \frac{\mathrm{D}\boldsymbol{v}}{\mathrm{D}t} = -\mathrm{grad}\, p + \mu \nabla^2 \boldsymbol{v} + \frac{1}{3}\mu\, \mathrm{grad}\, \mathrm{div}\, \boldsymbol{v} + \rho \boldsymbol{b}, \tag{5}$$

where grad denotes the spatial gradient operator, and $\nabla^2(\cdot) = \mathrm{div}[\mathrm{grad}(\cdot)^T]$ stands for the vector Laplace operator, with the superscript T denoting the tensor transpose.

A common approximation is to treat water as a barotropic fluid, for which the pressure is entirely determined by the fluid density. Adopting the pressure dependence on the density to be defined by

$$\frac{\mathrm{D}\rho}{\mathrm{D}t} = \frac{1}{c^2}\frac{\mathrm{D}p}{\mathrm{D}t}, \tag{6}$$

in which c is the speed of sound, and inserting the latter expression into (1), transforms the continuity equation into the form

$$\frac{\mathrm{D}p}{\mathrm{D}t} + K\, \mathrm{div}\, \boldsymbol{v} = 0, \tag{7}$$

where $K = \rho c^2$ is the fluid elastic compressibility modulus.

In order to complete the problem statement, initial and boundary conditions need to be specified. It is supposed that the fluid motion starts at time $t = 0$, and the fluid is at rest for $t \leq 0$; that is, the fluid velocities are then zero, $\boldsymbol{v} = 0$, and the stress in fluid is that of the hydrostatic pressure, $\boldsymbol{\sigma} = -p\boldsymbol{I}$. The boundary conditions which must be satisfied on the surfaces Γ_σ and Γ_v, see Fig. 1, are adopted in the following standard forms:

$$\begin{aligned} \boldsymbol{n}\cdot(\boldsymbol{\sigma}\boldsymbol{n}) = t_n \quad \text{and} \quad \boldsymbol{s}\cdot(\boldsymbol{\sigma}\boldsymbol{n}) = t_s \quad \text{on} \quad \Gamma_\sigma, \\ \boldsymbol{v}\cdot\boldsymbol{n} = v_n \quad \text{and} \quad \boldsymbol{v}\cdot\boldsymbol{s} = v_s \quad \text{on} \quad \Gamma_v, \end{aligned} \tag{8}$$

where t_n and t_s are prescribed traction vector components normal and tangential to the boundary Γ_σ, and v_n and v_s are prescribed velocity components normal and tangential to the boundary Γ_v. In most common situations, the boundary Γ_σ on which stresses are prescribed is that of the fluid free surface, here defined by $x_2 = h(x_1, t)$. Usually, the stresses within the fluid are measured relative to the atmospheric pressure, tacitly treated as constant. Hence, neglecting shear stresses on the free surface, the conditions prescribed on the fluid free surface can be simplified to the form

$$x_2 = h(x_1, t): \quad \boldsymbol{n}\cdot(\boldsymbol{\sigma}\boldsymbol{n}) = 0 \quad \text{and} \quad \boldsymbol{s}\cdot(\boldsymbol{\sigma}\boldsymbol{n}) = 0. \tag{9}$$

On the other hand, the boundary Γ_v, on which kinematic constraints are imposed, most often is identical with a fluid–solid interface. In the case of a rigid, fixed bottom, defined by $x_2 = f(x_1)$, the velocity vector component normal to the boundary is zero. As regards the velocity vector component tangential to the boundary, it is assumed that this component is not constrained. The latter simplification implies that the possible effects of the boundary layer along the bed are ignored; however, it is supposed that such viscous fluid flow effects are negligibly small in the case of water gravity waves. Accordingly, the kinematic boundary condition at the bed is expressed by

$$x_2 = f(x_1): \quad \boldsymbol{v} \cdot \boldsymbol{n} = 0. \tag{10}$$

On the moving parts of the solid boundaries, the kinematic conditions must be specified by prescribing in relation (10) the fluid/solid velocity components $v_n(x_1, x_2, t) \neq 0$.

The system of differential equations (5) and (7), complemented by relevant boundary conditions, describes the flow problem in terms of the pressure p and the velocity components v_i $(i = 1, 2)$. This set of equations is solved numerically by applying a discrete method presented in the next section.

3. Element-free Galerkin Methodology and Equations

The key issue in any meshless approach is the method used to evaluate, by interpolation or approximation, the values of field variables at any point of a domain by means of the corresponding values defined at a set of discrete nodes. Since the nodes can be distributed in an irregular, and sometimes highly disorderly, manner, the technique required for such evaluations is far from straightforward. This explains why the first techniques of this kind appeared only in the 1980s, and were initially devised for the needs of smooth curve and surface fitting for arbitrarily distributed data points. The successful data fitting algorithm was based on the moving least squares (MLS) approach. Its potential was fully realized in the field of applied mechanics only in the 1990s, when a group of first meshfree discrete methods, all implementing the MLS approximations, were developed. Examples of such methods include the diffuse element method (DEM) (Nayroles et al 1992), the EFG method (Belytschko et al 1995, 1996), and the partition of unity finite element method (PUFEM) (Melenk and Babuška 1996).

In the present work the EFG method is applied. The main ideas and important features of this method are illustrated in Figure 2. The continuum is represented by a set of discrete points, shown as the dots, at which the values of all field functions are defined. In order to evaluate the value of a field function at a spatial point $\boldsymbol{x}$, indicated by the square, a special weighting function, denoted by W in the figure, is used. This function is centred at the point $\boldsymbol{x}$ and vanishes at a distance R and farther from that point, see the circle of radius R. Therefore, only the data given at discrete points $\boldsymbol{x}_k$ inside the circular domain (the solid dots) are involved in the approximation of the field function at $\boldsymbol{x}$, while the data at the remaining nodes (the empty dots) do

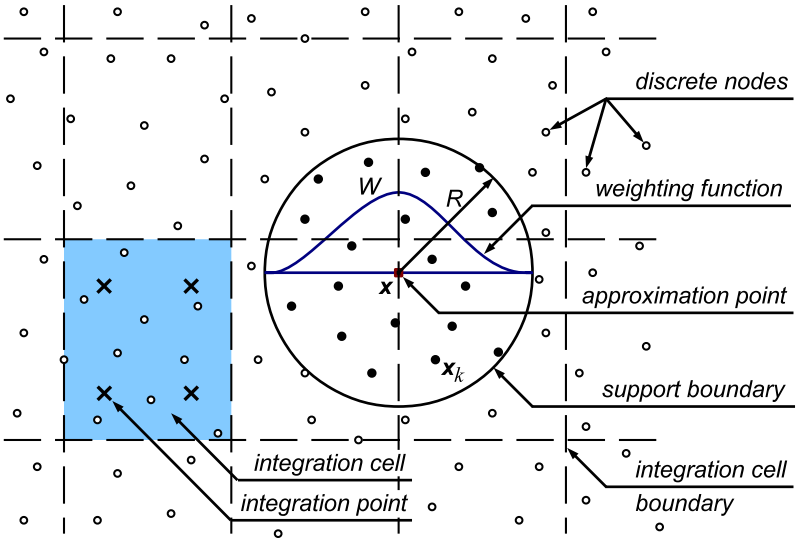

Fig. 2. The methods of approximation and integration of field functions in the EFG method. The approximation of a function at a point $\boldsymbol{x}$ involves parameters defined at discrete nodes (solid dots) situated within a circular domain of radius R centred at $\boldsymbol{x}$. The data at points outside this domain (empty dots) do not contribute to the approximation of the field function at the point $\boldsymbol{x}$. The integration of functions involved is carried out over background cells which are independent of the nodes distribution. Integration points within a cell are indicated by crosses

not contribute to the function evaluation at the point considered. In order to calculate integrals of approximated field functions appearing in the Galerkin formulation, background integration cells, with boundaries indicated by the dashed lines, are introduced. These integration cells, contrary to the standard finite element method, are completely independent of the layout of the discrete nodal points. Therefore, they can have simple shapes — most often rectangles or squares are used. Commonly, the integration is performed by applying the Gauss quadratures; the quadrature points are indicated in the figure by the crosses. Details regarding the integration technique in the EFG method can be found in the paper by Dolbow and Belytschko (1999).

In the moving least squares approach it is assumed that the approximation function is described by the relation

$$u(\boldsymbol{x}) \approx \hat{u}(\boldsymbol{x}) = \sum_{j=1}^{m} p_j(\boldsymbol{x})\, a_j(\boldsymbol{x}) = \boldsymbol{p}^T(\boldsymbol{x})\, \boldsymbol{a}(\boldsymbol{x}) \quad (j = 1, 2, \ldots, m), \tag{11}$$

where p_j are a set of m linearly independent functions which form a so-called basis, and a_j are unknown coefficients to be determined; the latter, as indicated above, are functions of the spatial coordinates. The functions $p_j(\boldsymbol{x})$ are usually assumed to be the polynomials, though other functions can be used if they model well the solution expected (for instance, in problems with singular solutions, singular functions can be included in the basis). In most applications, the functions p_j are chosen as a set of

monomials; these must include terms of the order which is sufficiently high to ensure approximation of all spatial derivatives appearing in the differential equation to be solved. For instance, in two-dimensional problems, the commonly used bases include the linear basis defined by

$$\boldsymbol{p}^T = (1 \quad x \quad z) \tag{12}$$

and the quadratic basis represented by

$$\boldsymbol{p}^T = \left(1 \quad x \quad z \quad x^2 \quad xz \quad z^2\right). \tag{13}$$

In the above expressions, x and z denote the plane rectangular coordinates, with the equivalence $x = x_1$ and $z = x_2$, see Fig. 1.

The unknown coefficients $a_j(\boldsymbol{x})$ $(j = 1, 2, \ldots, m)$ are determined by performing a least squares fit which minimizes the square of the distance between n values of the function u at the points $\boldsymbol{x}_k$ $(k = 1, 2, \ldots, n)$ and the corresponding local approximations $\hat{u}$ at the same points $\boldsymbol{x}_k$, as given by (11). Hence, the following weighted quadratic form is to be minimized:

$$J(\boldsymbol{x}) = \sum_{k=1}^{n} W(\boldsymbol{x} - \boldsymbol{x}_k) \left[\hat{u}(\boldsymbol{x}_k) - u(\boldsymbol{x}_k)\right]^2 . \tag{14}$$

The weighting function $W(\boldsymbol{x} - \boldsymbol{x}_k)$ which enters (14) is introduced in order to achieve the best fit at a given spatial point $\boldsymbol{x}$. This is ensured by choosing a special shape of the function W, which attains its maximum value at $\boldsymbol{x}$ and decreases monotonically in a smooth manner with increasing distance $r = |\boldsymbol{x} - \boldsymbol{x}_k|$ between the points $\boldsymbol{x}$ and $\boldsymbol{x}_k$. The weighting function is constructed in such a way that it is non-zero only in a small area called the compact support; most often, in the plane problems, the latter has a circular shape, as shown in Fig. 2. In this way the number of points $\boldsymbol{x}_k$ involved in the approximation of a field function u at the point $\boldsymbol{x}$ is limited. To make sure that the function W performs well in computations, it has to possess, apart from the afore-mentioned compactness, some additional properties (most importantly, it must be symmetric, i.e. $W(\boldsymbol{x} - \boldsymbol{x}_k) = W(\boldsymbol{x}_k - \boldsymbol{x})$, see Monaghan (1992), Liu and Liu (2003) and Li and Liu (2004). A few examples of the weighting functions are presented in Figure 3, in which R denotes the radius of the function circular support. These examples include the cubic, quartic and quintic (Wendland 1995) spline functions, and the exponential (Gaussian) function.

With the approximation formula (11) for $\hat{u}(\boldsymbol{x})$, the functional $J(\boldsymbol{x})$ in (14) becomes

$$J(\boldsymbol{x}) = \sum_{k=1}^{n} W(\boldsymbol{x} - \boldsymbol{x}_k) \left[\boldsymbol{p}^T(\boldsymbol{x}_k)\, \boldsymbol{a} - u(\boldsymbol{x}_k)\right]^2 , \tag{15}$$

which can be expressed in a compact matrix form (Nayroles et al 1992) as

$$J(\boldsymbol{x}) = (\boldsymbol{P}\, \boldsymbol{a} - \boldsymbol{u})^T\, \boldsymbol{W}(\Delta \boldsymbol{x})\, (\boldsymbol{P}\, \boldsymbol{a} - \boldsymbol{u}) . \tag{16}$$

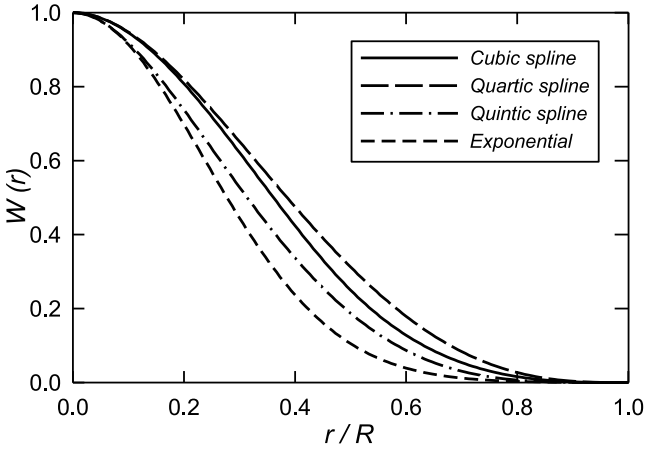

Fig. 3. Examples of weighting functions W

In (16), $\boldsymbol{u}$ is the vector containing all the nodal parameters $u_k = u(\boldsymbol{x}_k)$ $(k = 1, 2, \ldots, n)$, the matrix $\boldsymbol{P}$ is given by

$$\boldsymbol{P} = \begin{bmatrix} p_1(\boldsymbol{x}_1) & p_2(\boldsymbol{x}_1) & \cdots & p_m(\boldsymbol{x}_1) \\ p_1(\boldsymbol{x}_2) & p_2(\boldsymbol{x}_2) & \cdots & p_m(\boldsymbol{x}_2) \\ \vdots & \vdots & \ddots & \vdots \\ p_1(\boldsymbol{x}_n) & p_2(\boldsymbol{x}_n) & \cdots & p_m(\boldsymbol{x}_n) \end{bmatrix}, \tag{17}$$

and $\boldsymbol{W}(\Delta \boldsymbol{x})$ is the diagonal matrix defined by

$$\boldsymbol{W}(\Delta \boldsymbol{x}) = \begin{bmatrix} W(\boldsymbol{x} - \boldsymbol{x}_1) & 0 & \cdots & 0 \\ 0 & W(\boldsymbol{x} - \boldsymbol{x}_2) & \cdots & 0 \\ \vdots & \vdots & \ddots & \vdots \\ 0 & 0 & \cdots & W(\boldsymbol{x} - \boldsymbol{x}_n) \end{bmatrix}. \tag{18}$$

The functional $J(\boldsymbol{x})$ defined by (16) is stationary (attains its minimum value) when its all derivatives with respect to the coefficients a_j $(j = 1, 2, \ldots, m)$ are zero. This yields

$$\frac{\partial J(\boldsymbol{x})}{\partial \boldsymbol{a}} = 0 \quad \Rightarrow \quad \boldsymbol{A}(\boldsymbol{x})\, \boldsymbol{a}(\boldsymbol{x}) - \boldsymbol{B}(\boldsymbol{x})\, \boldsymbol{u} = \boldsymbol{0}, \tag{19}$$

where

$$\boldsymbol{A} = \boldsymbol{P}^T \boldsymbol{W}(\Delta \boldsymbol{x})\, \boldsymbol{P}, \quad \boldsymbol{B} = \boldsymbol{P}^T \boldsymbol{W}(\Delta \boldsymbol{x}). \tag{20}$$

For the particular case of the plane problem and the polynomial basis $\boldsymbol{p}(\boldsymbol{x})$ reduced to the linear form defined by (12) ($m = 3$), the matrix $\boldsymbol{A}$ of dimensions 3×3 is expressed by the relation

$$\boldsymbol{A}(\boldsymbol{x}) = \sum_{k=1}^{n} W(\boldsymbol{x} - \boldsymbol{x}_k)\, \boldsymbol{p}(\boldsymbol{x}_k)\, \boldsymbol{p}^T(\boldsymbol{x}_k) = \sum_{k=1}^{n} W(\boldsymbol{x} - \boldsymbol{x}_k) \begin{bmatrix} 1 & x_k & z_k \\ x_k & x_k^2 & x_k z_k \\ z_k & x_k z_k & z_k^2 \end{bmatrix}, \tag{21}$$

and the k-th column of the matrix $\boldsymbol{B}$ of dimensions $3 \times n$ is given by

$$\boldsymbol{B}_k(\boldsymbol{x}) = W(\boldsymbol{x} - \boldsymbol{x}_k)\, \boldsymbol{p}(\boldsymbol{x}_k) = W(\boldsymbol{x} - \boldsymbol{x}_k) \begin{pmatrix} 1 \\ x_k \\ z_k \end{pmatrix} \quad (k = 1, 2, \ldots, n). \tag{22}$$

The conditioning, and the invertibility, of the matrix $\boldsymbol{A}$ depends on the number k and the relative arrangement of the nodal points $\boldsymbol{x}_k$ involved in the approximation at $\boldsymbol{x}$. A necessary condition for non-singularity of $\boldsymbol{A}$ is that at least m points are used for the approximation at a given spatial point $\boldsymbol{x}$, and that the points $\boldsymbol{x}_k$ are not all located on a straight line.

Solution of the matrix equation (19) determines the required coefficients a_j which minimize the functional $J(\boldsymbol{x})$ as

$$\boldsymbol{a}(\boldsymbol{x}) = \boldsymbol{A}^{-1}(\boldsymbol{x})\, \boldsymbol{B}(\boldsymbol{x})\, \boldsymbol{u}. \tag{23}$$

The above solution for $\boldsymbol{a}$ depends continuously on the position $\boldsymbol{x}$ of a point selected for the fit by the moving least squares algorithm. Returning now to equation (11) and inserting into it the expression for $\boldsymbol{a}$, one obtains the formula for approximation of the function $u(\boldsymbol{x})$ in the following form

$$\hat{u}(\boldsymbol{x}) = \sum_{k=1}^{n} N_k(\boldsymbol{x})\, u_k, \tag{24}$$

where N_k are the shape functions. The latter are given by

$$N_k(\boldsymbol{x}) = \boldsymbol{p}^T(\boldsymbol{x}) \boldsymbol{A}^{-1}(\boldsymbol{x})\, \boldsymbol{B}_k(\boldsymbol{x}), \tag{25}$$

and define interpolation functions for each nodal value $\hat{u}_k$; recall that the vectors $\boldsymbol{B}_k$ are given by (22). In general, the EFG shape functions do not possess the Kronecker delta property, that is $N_i(\boldsymbol{x}_k) \neq \delta_{ik}$, which is the case for the FE shape functions. This is due to the fact that the functions N_k are established here by the optimization scheme, so that, in general, the local values of the approximating function $\hat{u}_k$ do not exactly fit the nodal unknown values u_k.

In order to solve differential equations of mechanics by a discrete method, one also needs spatial derivatives of the MLS shape functions, necessary to approximate the

gradient of $\hat{u}(\boldsymbol{x})$ given by equation (24). To construct the derivatives of the functions N_k, let rewrite relation (25) in the form

$$N_k(\boldsymbol{x}) = \boldsymbol{p}^T(\boldsymbol{x})\boldsymbol{C}_k(\boldsymbol{x}) \quad (k = 1, 2, \ldots, n), \tag{26}$$

with the vector $\boldsymbol{C}_k$ of length m defined by

$$\boldsymbol{C}_k(\boldsymbol{x}) = \boldsymbol{A}^{-1}(\boldsymbol{x})\,\boldsymbol{B}_k(\boldsymbol{x}). \tag{27}$$

Then, the derivative of the shape function N_k with respect to the spatial coordinate x_i $(i = 1, 2)$ is given by

$$\frac{\partial N_k}{\partial x_i} = \frac{\partial \boldsymbol{p}^T}{\partial x_i}\,\boldsymbol{C}_k + \boldsymbol{p}^T\boldsymbol{A}^{-1}\left(\frac{\partial \boldsymbol{B}_k}{\partial x_i} - \frac{\partial \boldsymbol{A}}{\partial x_i}\,\boldsymbol{C}_k\right), \tag{28}$$

where

$$\frac{\partial \boldsymbol{A}}{\partial x_i} = \sum_{k=1}^{n} \frac{\partial W(\boldsymbol{x} - \boldsymbol{x}_k)}{\partial x_i}\,\boldsymbol{p}(\boldsymbol{x}_k)\,\boldsymbol{p}^T(\boldsymbol{x}_k) \tag{29}$$

and

$$\frac{\partial \boldsymbol{B}_k}{\partial x_i} = \frac{\partial W(\boldsymbol{x} - \boldsymbol{x}_k)}{\partial x_i}\,\boldsymbol{p}(\boldsymbol{x}_k). \tag{30}$$

In a similar way, higher-order derivatives of the MLS shape functions can be calculated, but these are not necessary in the present work.

Having determined the functions N_k and their derivatives, needed to approximate field functions and their derivatives in terms of the nodal parameters u_k, one can now proceed to discretization of the problem that is described by the Navier-Stokes and continuity equations. It turns out that for the EFG method this step is quite similar to the standard finite element method. Accordingly, the differential equations (5) and (7) are multiplied by a set of weighting functions and then integrated over the whole domain occupied by the fluid, leading to the weak formulation of the problem. As is characteristic of the Galerkin method, the latter weighting functions are identical to the shape functions N_k; that is, they are different from the weighting functions W used for the MLS approximations of the field variables. Next, the formula (24) is employed in the equations to express continuous field function derivatives in terms of the shape functions derivatives and the discrete nodal parameters u_k. Then, Green's theorem is applied to lower by one the order of differentiation of the functions involved. The above procedure transforms the problem to the solution of a set of differential equations which, in a matrix notation, takes the form:

$$\boldsymbol{G}\dot{\boldsymbol{u}}(t) + \boldsymbol{K}\boldsymbol{u}(t) = \boldsymbol{f}(t), \quad \boldsymbol{u}(0) = \boldsymbol{u}_0. \tag{31}$$

In the latter expression, $\boldsymbol{u}$ is the vector of unknown discrete values comprising the velocities and pressures in all discrete nodes of the system, $\boldsymbol{f}$ is the loading vector,

and $\boldsymbol{u}_0$ represents the initial solution vector (nodal values of the velocity and pressure fields at time $t = 0$).

The matrices $\boldsymbol{G}$ and $\boldsymbol{K}$ and the vector $\boldsymbol{f}$ result from the calculation of integrals of respective terms involving the shape functions and their first derivatives. These matrices must be aggregated at each time step, as the spatial distribution of the discrete nodes continually changes during the fluid flow. In order to integrate the equations (31), a single-step scheme, known as the weighted average θ-method, has been employed (Zienkiewicz and Taylor 2000). Application of this method to (31) gives the following system of algebraic equations:

$$(\boldsymbol{G} + \Delta t\,\theta \boldsymbol{K})\,\boldsymbol{u}_{i+1} = [\boldsymbol{G} - \Delta t\,(1-\theta)\boldsymbol{K}]\,\boldsymbol{u}_i + \Delta t \bar{\boldsymbol{f}}_i \quad (i = 0, 1, 2, \ldots), \tag{32}$$

which connects the solution vectors $\boldsymbol{u}_i$ and $\boldsymbol{u}_{i+1}$ at two successive time levels, t_i and $t_{i+1} = t_i + \Delta t$, where Δt denotes the time step length. The vector $\bar{\boldsymbol{f}}_i$ appearing in (32) is the time-averaged loading vector which, assuming its linear variation during the current time step i, is expressed by

$$\bar{\boldsymbol{f}}_i = (1-\theta)\boldsymbol{f}_i + \theta \boldsymbol{f}_{i+1}. \tag{33}$$

The value of the weighting parameter θ can vary between zero (fully explicit Euler scheme) and unity (fully implicit backward scheme). The most accurate results are obtained for $\theta = 0.5$, but the best numerical stability is usually achieved for $\theta \sim 1$.

4. Numerical Simulations

The discrete method, presented in the preceding section, has been applied to simulate the propagation of free-surface gravity waves in water over beds of simple geometry. The following parameters have been used to describe the physical properties of water: the reference density (at the atmospheric pressure) $\rho_0 = 10^3$ kg m^{-3}, the fluid shear viscosity $\mu = 1.01 \times 10^{-3}$ Ns m^{-2}, and the compressibility modulus $K = 2.04 \times 10^9$ Pa; both μ and K have been treated as constants.

First, in order to validate the numerical model, the wave propagation in water of uniform depth has been considered. Hence, the geometry typical of a wave flume has been adopted, see Figure 4, and the predictions of the EFG model have been compared with results of a laboratory experiment carried out by Szmidt and Hedzielski (2007). In that experiment, the movement of water, of an initial depth of $H = 0.6$ m, was induced by oscillatory translations of a vertical wall AB, carried out with an angular frequency of 2.90 s^{-1} (equivalent to a period of 2.17 s, generating a surface wave of a length of 4.80 m = 8 H, travelling with a phase velocity of 2.22 m s^{-1}. The walls AD and CD are treated as fixed and rigid. For the purpose of comparisons, a set of measurements of the variation of the free-surface elevation at a distance of 3 m from the wave-maker wall has been used.

The EFG model was driven by the horizontal velocities calculated from the corresponding displacements measured at the wave-maker wall during the experiment.

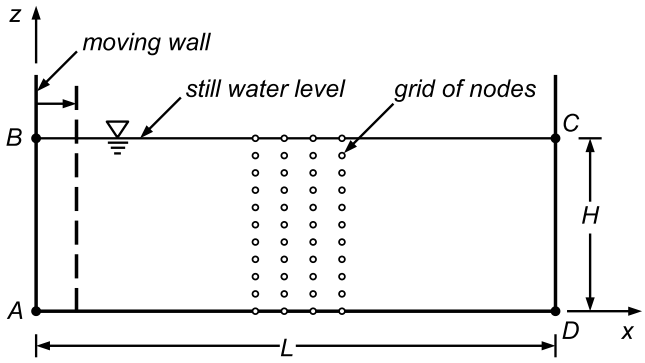

Fig. 4. Initial water domain geometry for a flow in a wave flume

The length of the computational domain was $L = 15$ m. A uniform grid of discrete nodes used in these test simulations consisted of 11 'rows' of nodes along the vertical and 101 'columns' of nodes along the horizontal axis, so that the initial vertical and horizontal spacings were equal to 6 cm and 15 cm, respectively. In total, the discrete system consisted of 1111 nodes. The spacial integration by the Gaussian quadratures was carried out on background rectangular cells, the vertices of which coincided with the initial positions of the discrete nodes; hence, their dimensions were 6 cm × 15 cm. In each cell four quadrature points were used. The time integration was performed with the time step $\Delta t = 5 \times 10^{-3}$ s, which corresponds, for the initial, undistorted grid of nodes, to the Courant number of about 0.07. The numerical and experimental results are compared in Figure 5. The plot in Fig. 5a displays the time history of the horizontal displacements of the wave-maker, and the plots in Fig. 5b illustrate the evolution of the free-surface elevation at the chosen point at 3 m from the generator, with the solid line representing the EFG model predictions, and the dashed line with the circles showing the experimental data. The plots demonstrate a good agreement between the numerical and experimental results. The numerically predicted wave length compares well with that measured in the flume. There are some differences between the calculated and actually measured free-surface elevations, but these are small — the maximum relative differences for the crest elevations are about 2%, and those for the troughs are about 3%. Therefore, on the basis of these results, it can be concluded that the EFG model is constructed properly and gives results of satisfactory accuracy.

Next, the numerical model has been used to simulate a transient problem of wave propagation in water of variable depth. For this purpose, two cases of beds with sloping sections have been considered, to mimic idealized beach profiles. The first case, sketched in Fig. 6a, represents a uniformly inclined beach, with a slope $1/m$, ending at a vertical wall, and the second case, depicted in Fig. 6b, represents a uniformly inclined beach followed by a flat, constant-depth region. In both cases, a free-surface wave is supposed to be generated by a movement of a rigid vertical wall situated at the left-hand end of the flow domain (that is, at $x = 0$). The geometric dimensions of the

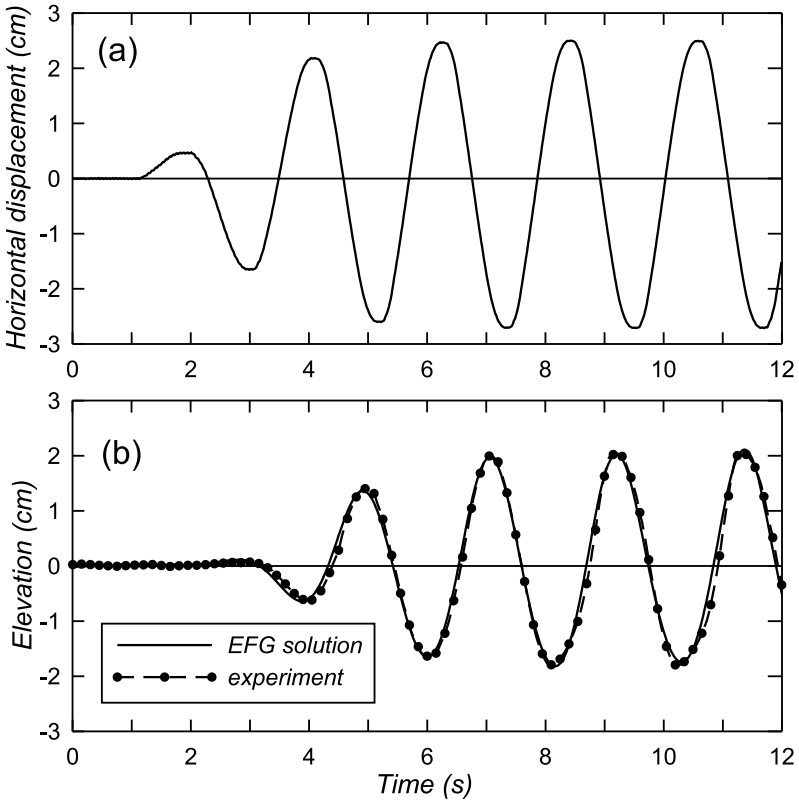

Fig. 5. Comparison of the EFG model predictions with experimental data: (a) time variation of the wave-maker horizontal displacements, (b) time variation of the free-surface elevation at the distance of 3 m from the wave-maker

problem have been adopted as those of a wave flume. Hence, the region adjacent to the moving wall, of a length L_1, has a constant depth $H = 0.6$ m, and the total length of the water domain, in both cases, is $L = 15$ m.

It has been assumed that water is at rest at times $t < 0$, and is set in motion by the vertical wall which, starting at $t = 0$, makes a single translational movement in the horizontal direction by a distance of D_0, and then stops. The following smooth function, with continuous first and second-order time derivatives at $t = 0$, has been adopted to describe the horizontal displacement $d_0(t)$ of the wave-maker:

$$d_0(t) = D_0 \left[1 - \exp\left(-\tau^3\right)\right], \quad \tau = \frac{t}{T_0}, \tag{34}$$

where T_0 is a characteristic time of the wave-maker movement.

The discrete grid imposed on the water domain consisted of 11 'rows' of nodes along the vertical, and 251 'columns' of nodes along the horizontal direction. The spacing of nodal points was constant along the length of the flume and was equal to 6 cm, while in the vertical direction the spacing of nodes, at each x uniformly

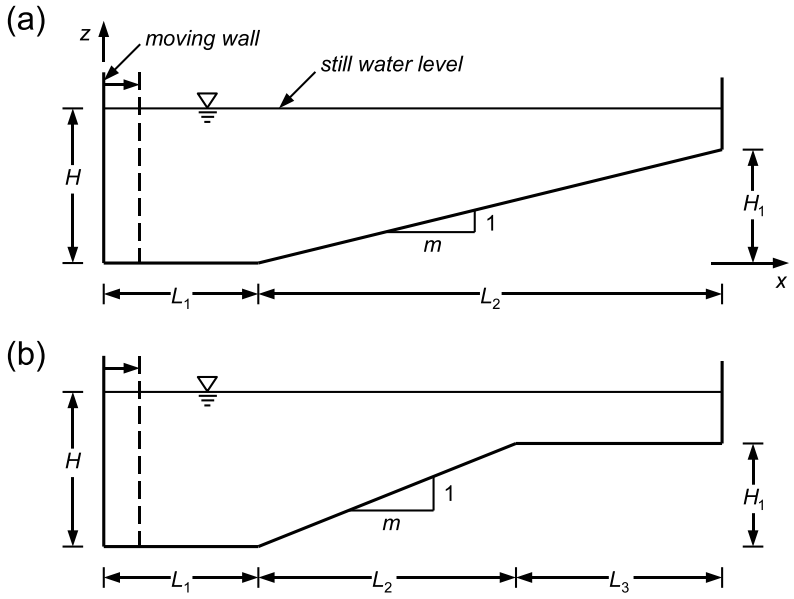

Fig. 6. Profiles of two beds with sloping sections

distributed along z, depended on the local depth of water (the largest vertical spacing, in the region of constant depth equal to H, was 6 cm). The time integration of the problem equations was performed by using a constant-length time increment $\Delta t = 10^{-3}$ s. Such a relatively short time step was necessary to maintain stability of the numerical scheme.

The plots in Figure 7 illustrate the transformation of a wave travelling over (a) the horizontal bed, and (b) over the sloping bed displayed in Fig. 6a. In the latter case, the geometric dimensions are $L_1 = 3$ m, $L_2 = 12$ m and $H_1 = 40$ cm, so that the slope of the uniformly inclined section of the bed is 1/30, and the minimum depth of still water is equal to 20 cm at $x = 15$ m. The wave motion has been induced by moving the rigid wall at $x = 0$ by a distance of $D_0 = 20$ cm, with the characteristic time $T_0 = 1.0$ s. The plots in Fig 7a, presenting the evolution of a transient wave over the horizontal bottom, show a steady decrease in the leading wave crest height with an increasing propagation distance. Contrary to that, the wave propagating over the shoaling bed, see Fig 7b, retains approximately the same height over the inclined section of the bed (i.e., for $x \geq 3$ m). This means, in the particular case considered here, that the shoaling and dispersive effects are roughly counter-balanced. Also, an effect of the sloping bed on the wave length is apparent in Fig 7b, as the shortening and steepening of the wave profile are clearly visible in the plots.

Finally, Figure 8 shows the transformation of a wave propagating over the bed defined in Fig. 6b. Two different slopes, 1/15 and 1/10, of the inclined bottom section have been considered, in order to examine how the bed sloping affects the wave be-

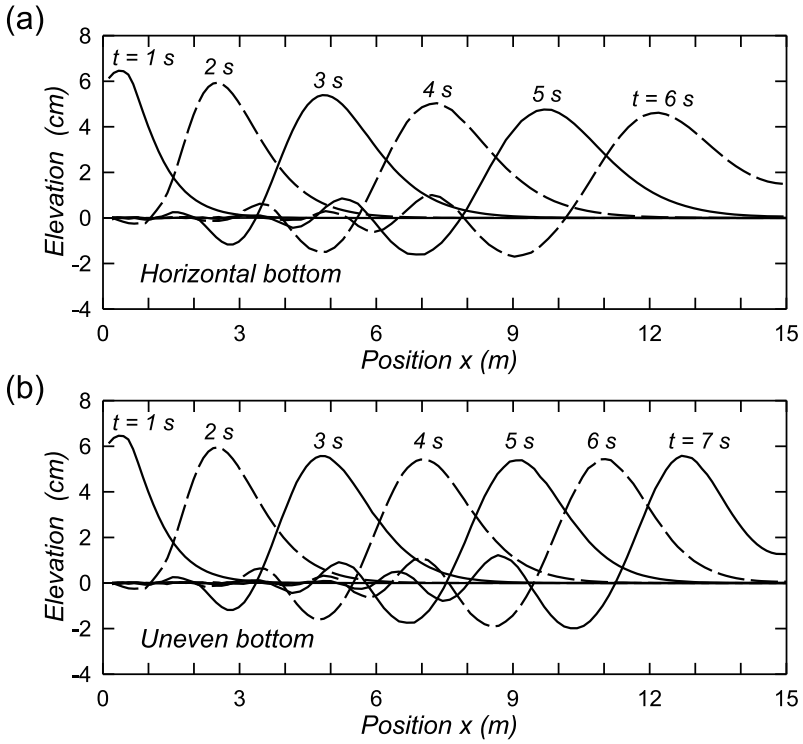

Fig. 7. Evolution of the free-surface elevation for a transient wave propagating: (a) over the horizontal bed, (b) over the uneven bed defined in Fig. 6a (D_0 = 20 cm, T_0 = 1.0 s)

haviour. Again, L_1 = 3 m and H_1 = 40 cm, so that the inclined bed extends between the points x = 3 and x = 9 m in the case of the smaller slope, and between x = 3 and x = 7 m in the case of the larger slope. Once again some increase in the wave front height, as the wave passes through the shoaling zone, can be observed, and the wave length shortening occurring over the sloping bed is clearly seen in the plots.

Exactly the same bed configuration as defined in Fig. 6b and its effect on the gravity wave transformation was analysed earlier in the paper by Staroszczyk (2009), in which the standard finite element method was employed to construct the numerical model. The FE results, obtained for the same wave excitation parameters (D_0 and T_0 in equation (34)) as adopted here for the EFG calculations, are presented for comparison in Fig. 8b, see the solid circles. For the sake of clarity of the plots, the FE results are displayed only for the time instants 2, 5 and 8 s. About the same initial distribution of the discrete nodal points in both, EFG and FE, models was used. It is seen that both methods, EFG and FE, give similar results, with relative discrepancies between the model predictions not exceeding 3% for the leading wave crest heights. This proves that the EFG model delivers reliable results.

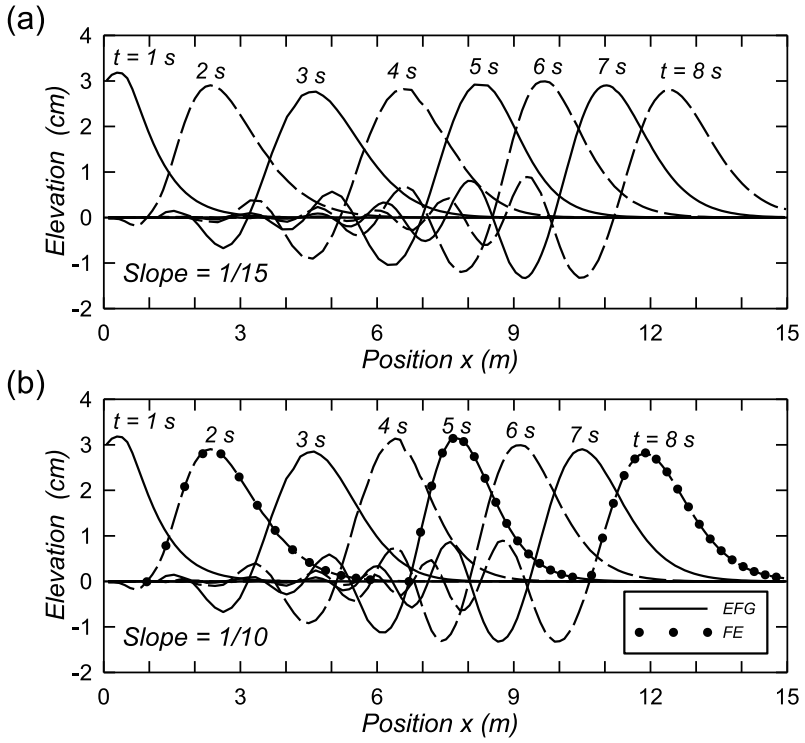

Fig. 8. Evolution of the free-surface elevation for a transient wave propagating over the bed defined in Fig. 6b, for the slopes 1/15 and 1/10 of the inclined section of the bed (D_0 = 10 cm, T_0 = 1.0 s). For comparison, shown are also results from the FE model (solid circles)

5. Conclusions

An element-free Galerkin model has been constructed to investigate the plane problem of free-surface wave propagation in water of variable depth. The discrete model has been used to simulate the transformation of transient gravity waves travelling over the bottom of simple shape, with the focus on the wave profile evolution over a sloping bed. The numerical model reproduces the free-surface elevations measured in a wave flume with a satisfactory level of accuracy. The results obtained for uneven beds, with gentle and moderate slopes, have demonstrated the method's capability of dealing with problems involving moving boundaries and non-linear effects associated with the free-surface wave propagation in water of non-uniform depth.

The comparison of the predictions of the EFG model with those obtained by applying the conventional finite element approach has shown that, for approximately the same resolution of discrete nodes, the numerical performance of the two methods, EFG and FE, is similar, with a small gain in accuracy achieved in the case of the EFG approach. However, the EFG method is more difficult to implement in a computer code due to its increased complexity compared to the classical FEM (for which

many effective algorithms have been developed over the decades). For this reason, it seems that for conventional water wave propagation problems, in which no surfaces of discontinuity develop in the fluid (there is no fluid fragmentation), it is more effective to use the typical finite element approach. On the contrary, when discontinuity surfaces develop and evolve within the fluid body (for instance, in such phenomena as wave breaking or wave impact at a wall), then the application of the element-free Galerkin method may be preferred, despite its increased computational cost, as this method is particularly well suited to coping with problems in which fragmentation of the medium takes place.

References

Antoci C., Gallati M. and Sibilla S. (2007) Numerical simulation of fluid–structure interaction by SPH, *Comput. Struct.*, **85** (11–14), 879–890, DOI: 10.1016/j.compstruc.2007.01.002.

Belytschko T., Krongauz Y., Dolbow J. and Gerlach C. (1998) On the completeness of meshfree particle methods, *Inter. J. Numer. Meth. Eng.*, **43** (5), 785–819, DOI: 10.1002/(SICI)1097-0207(19981115)43:5.

Belytschko T., Krongauz Y., Organ D., Fleming M. and Krysl P. (1996) Meshless methods: An overview and recent developments, *Comput. Meth. Appl. Mech. Eng.*, **139** (1–4), 3–47.

Belytschko T., Lu Y. Y. and Gu L. (1995) Crack propagation by element-free Galerkin methods, *Eng. Fracture Mech.*, **51** (2), 295–315.

Chadwick P. (1999) *Continuum Mechanics: Concise Theory and Problems*, Dover, Mineola, New York, 2nd edn.

Dalrymple R. A. and Rogers B. D. (2006) Numerical modeling of water waves with the SPH method, *Coastal Eng.*, **53** (2–3), 141–147, DOI: 10.1016/j.coastaleng.2005.10.004.

Dingemans M. W. (1997) *Water Wave Propagation over Uneven Bottoms*, World Scientific, Singapore.

Dolbow J. and Belytschko T. (1999) Numerical integration of the Galerkin weak form in meshfree methods, *Comput. Mech.*, **23** (3), 219–230.

Gingold R. A. and Monaghan J. J. (1977) Smoothed particle hydrodynamics: theory and application to non-spherical stars, *Mon. Not. R. Astron. Soc.*, **181**, 375–389.

Gómez-Gesteira M., Cerqueiro D., Crespo C. and Dalrymple R. A. (2005) Green water overtopping analyzed with a SPH method, *Ocean Eng.*, **32** (2), 223–238, DOI: 10.1016/j.oceaneng.2004.08.003.

Li S. and Liu W. K. (2004) *Meshfree Particle Methods*, Springer, Berlin.

Liu G. R. and Liu M. B. (2003) *Smoothed Particle Hydrodynamics: A Meshfree Particle Method*, World Scientific, Singapore.

Lo E. Y. M. and Shao S. (2002) Simulation of near-shore solitary wave mechanics by an incompressible SPH method, *Appl. Ocean Res.*, **24** (5), 275–286, DOI: 10.1016/S0141-1187(03)00002-6.

Löhner R., Sacco C., Oñate E. and Idelsohn S. (2002) A finite point method for compressible flow, *Int. J. Numer. Meth. Eng.*, **53** (8), 1765–1779.

Lucy L. B. (1977) A numerical approach to the testing of the fission hypothesis, *Astron. J.*, **82** (12), 1013–1024.

Melenk J. M. and Babuška I. (1996) The partition of unity finite element method: Basic theory and applications, *Comput. Meth. Appl. Mech. Eng.*, **139** (1–4), 289–314.

Monaghan J. J. (1992) Smoothed particle hydrodynamics, *Annu. Rev. Astron. Astrophys.*, **30**, 543–574, DOI: 10.1146/annurev.aa.30.090192.002551.

Nayroles B., Touzot G. and Villon P. (1992) Generalizing the finite element method: diffuse approximation and diffuse elements, *Comput. Mech.*, **10** (5), 307–318.

Oñate E., Idelsohn S. R., Zienkiewicz O. C. and Taylor R. L. (1996a) A finite point method in computational mechanics. Applications to convective transport and fluid flow, *Int. J. Numer. Meth. Eng.*, **39** (22), 3839–3866.

Oñate E., Idelsohn S. R., Zienkiewicz O. C., Taylor R. L. and Sacco C. (1996b) A stabilized finite point method for analysis of fluid mechanics problems, *Comput. Meth. Appl. Mech. Eng.*, **139** (1–4), 315–346.

Ortega E., Oñate E. and Idelsohn S. (2007) An improved finite point method for tridimensional potential flows, *Comput. Mech.*, **40** (6), 949–963.

Staroszczyk R. (2009) A Lagrangian finite element analysis of gravity waves in water of variable depth, *Arch. Hydro-Eng. Environ. Mech.*, **56** (1–2), 43–61.

Stoker J. J. (1957) *Water Waves. The Mathematical Theory with Applications*, Inter-Science, New York.

Szmidt K. and Hedzielski B. (2007) On the transformation of long gravitational waves in a region of variable water depth: a comparison of theory and experiment, *Arch. Hydro-Eng. Environ. Mech.*, **54** (2), 137–158.

Wehausen J. V. and Laitone E. V. (1960) Surface waves. In: *Encyclopedia of Physics* (ed. S. Flügge), vol. IX, Springer, Berlin, 446–778.

Wendland H. (1995) Piecewise polynomial, positive definite and compactly supported radial functions of minimal degree, *Adv. Comput. Math.*, **4** (1), 389–396.

Zienkiewicz O. C. and Taylor R. L. (2000) *The Finite Element Method. The Basis*, vol. 1. Butterworth-Heinemann, Oxford, 5th edn.